




Correlated negative magnetization, exchange bias, and electrical properties in $\text{La}_{1-x}\text{Pr}_x\text{CrO}_3$ Deepak, A. Kumar , A. K. Bera, and S. M. Yusuf **Solid State Physics Division, Bhabha Atomic Research Centre, Mumbai 400085, India
and Homi Bhabha National Institute, Anushaktinagar, Mumbai 400094, India* (Received 2 April 2022; accepted 5 July 2022; published 22 July 2022)

In the present work, we report the correlations among negative magnetization (NM), exchange bias (EB), and electrical properties in $\text{La}_{1-x}\text{Pr}_x\text{CrO}_3$ ($x = 0, 0.25, 0.5, 0.75, \text{ and } 1$) compounds using dc magnetization, neutron depolarization, neutron diffraction, and impedance spectroscopy. The dc magnetization study infers the negative magnetization (NM) phenomenon in $x = 0.25, 0.5, \text{ and } 0.75$ compounds, where the compensation temperature (T_{COMP}) increases with x . At low temperature ($T < T_{\text{COMP}}$), these compounds exhibit NM along with positive EB, indicating a correlation between the negative polarity of magnetization and the positive polarity of EB. However, the end compound $x = 0$ does not show any NM and/or EB, whereas the other end compound, $x = 1$, shows a negative EB without any NM. The presence or absence of magnetization reversal has been explained within the framework of Cooke's model which involves a competition between antiparallel coupled canted Cr^{3+} and polarized Pr^{3+} moments. Interestingly, maximum ac conductivity (with minimum activation energy required for conduction) at $x = 0.75$ (which exhibits maximum T_{COMP}) is found entangled with the lattice parameters' crossover from $a < c$ to $a > c$ around $x = 0.75$, as evident from the neutron diffraction study. The physics behind the polarity reversals of magnetization and EB, and its close connection with electrical properties, has been understood by employing the macroscopic, mesoscopic, and microscopic experimental techniques. Such correlated physical properties make these compounds useful for making thermomagnetic switches and thermal-assisted magnetic random access memory.

DOI: [10.1103/PhysRevMaterials.6.074405](https://doi.org/10.1103/PhysRevMaterials.6.074405)

I. INTRODUCTION

Rare-earth (R) orthochromites, $R\text{CrO}_3$, have been investigated in the past few decades due to their interesting physical properties and potential applications in many conventional devices such as catalytic converters [1], solid-oxide fuel cell [2], and gas sensors [3]. LaCrO_3 , the first member of this series of compounds, has been widely investigated in nano- and bulk crystalline forms because of its fascinating electrical and chemical properties [4–6]. A magnetic phase transition occurs in this compound at the Néel temperature (T_N) ~ 290 K [7], where the compound orders into a canted antiferromagnetic (CAFM) spin configuration. The magnetic properties of this compound can be tuned by magnetic rare-earth (R) substitution at the La site in $\text{La}_{1-x}R_x\text{CrO}_3$. With the magnetic R^{3+} ion, these compounds possess additional $R^{3+}\text{-Cr}^{3+}$ and $R^{3+}\text{-R}^{3+}$ magnetic interactions along with $\text{Cr}^{3+}\text{-Cr}^{3+}$. These extra interactions could bring unusual phenomena, such as negative magnetization (NM) [8,9] and exchange bias (EB) [10], in these compounds. For instance: the NM phenomenon has been reported for $\text{La}_{1-x}\text{Ce}_x\text{CrO}_3$ ($x = 0.9$ and 1) [11], $\text{La}_{0.5}\text{Gd}_{0.5}\text{CrO}_3$ [12], and $\text{La}_{0.75}\text{Nd}_{0.25}\text{CrO}_3$ [13] compounds; however, this phenomenon is absent in the LaCrO_3 compound [14]. The compounds showing the NM phenomenon could be exploited to make thermomagnetic switches [15]. Besides NM, the polarity reversal of EB is currently an active area of

research in magnetism, because compounds show this interesting feature is useful for making thermal-assisted magnetic random access memory [16]. In the literature, EB with the same polarity, either positive or negative, is reported in various compounds, viz., $\text{Dy}_{1-x}\text{Nd}_x\text{CrO}_3$ [17], $\text{LaCr}_{0.5}\text{Fe}_{0.5}\text{O}_3$ [18], $\text{Nd}_{1-x}\text{Eu}_x\text{CrO}_3$ [19], and $\text{Sm}_{0.4}\text{Ca}_{0.6}\text{MnO}_3$ [20], whereas sign reversal of EB as a function of temperature is reported in a few studies [21,22]. In the literature, not much attention is given to study the variation of EB with composition (x) in a $\text{La}_{1-x}R_x\text{CrO}_3$ series of compounds and its correlation with the NM. With this primary motivation, in the present study, we have chosen Pr^{3+} substituted $\text{La}_{1-x}\text{Pr}_x\text{CrO}_3$ ($x = 0, 0.25, 0.5, 0.75, \text{ and } 1$) compounds. The dc magnetization study on $\text{La}_{1-x}\text{Pr}_x\text{CrO}_3$ ($0 \leq x \leq 1$) inferred the NM over $x = 0.2$ to 0.85 of Pr^{3+} concentration [14] and EB for $x = 0.7$ to 0.85 [23]. A neutron diffraction (ND) study on the $x = 0.5$ [14,24] and 1 [25] compounds revealed a G -type antiferromagnetic ordering of Cr^{3+} in these compounds. In the present paper, we bring out correlations among NM, EB, and electrical properties for the $x = 0, 0.25, 0.5, 0.75, \text{ and } 1$ compounds. The work highlights the usefulness of microscopic neutron diffraction and mesoscopic neutron depolarization techniques to establish the magnetism of these interesting Pr substituted $\text{La}_{1-x}\text{Pr}_x\text{CrO}_3$ compounds.

In the present study, we report the polarity reversals of NM and EB, and correlated electrical properties in compounds of $\text{La}_{1-x}\text{Pr}_x\text{CrO}_3$ ($x = 0, 0.25, 0.5, 0.75, \text{ and } 1$) series using dc magnetization and impedance spectroscopy studies. Moreover, we have employed the microscopic ND technique to

*smyusuf@barc.gov.in

understand the physics of correlation among different physical properties of these compounds. The dc magnetization study infers that $x = 0.25, 0.5$, and 0.75 compounds exhibit the NM, and positive EB (at $T < T_{\text{COMP}}$), indicating a correlation between these two phenomena. On the other hand, the negative EB is observed for the $x = 1$ compound whose magnetization remains positive for all temperatures below the T_N . The maximum T_{COMP} and ac conductivity (derived from the impedance spectroscopy) are found for the $x = 0.75$ compound, which have been explained in terms of Cooke's model and lattice parameters' crossover from $a < c$ to $a > c$ (derived from the ND) across $x = 0.75$, respectively. Thus, the present study on $\text{La}_{1-x}\text{Pr}_x\text{CrO}_3$ compounds has established correlations among NM and EB in a series of compounds, which makes these useful for spintronics applications.

II. EXPERIMENTAL DETAILS

The polycrystalline compounds $\text{La}_{1-x}\text{Pr}_x\text{CrO}_3$ ($x = 0, 0.25, 0.5, 0.75$, and 1) were prepared by the solid-state reaction method using La_2O_3 , Pr_2O_3 , and Cr_2O_3 as starting chemicals. Stoichiometric amounts of these chemicals were mixed using a mortar and pestle and ground together for 1–2 h. Afterward, the mixture of these chemicals was pressed into a cylindrical pellet and sintered in air at 1400°C for 24 h. This sintering was repeated twice for each compound. Structural characterization was performed by using x-ray and temperature-dependent ND. X-ray diffraction patterns were recorded using lab source-based $\text{Cu-K}\alpha$ radiation. The ND experiment was carried out at Powder Diffractometer-I ($\lambda = 1.094 \text{ \AA}$), Dhruva reactor, Mumbai, India. All diffraction patterns were analyzed by the Rietveld refinement method [26] using the FULLPROF computer program [27]. Here we mention that in all diffraction patterns, the x axis is plotted as the magnitude of the momentum transfer, $Q = 4\pi \sin\theta/\lambda$, where λ is the wavelength of the radiation used and θ is half of the scattering angle (2θ). Scanning electron microscopy (SEM) and energy dispersive x-ray spectroscopy (EDX) (using Carl Zeiss, GEMINISEM 300) were used to study microstructure and elemental composition of the compounds, respectively. Temperature- and magnetic-field-dependent dc magnetization measurements were carried out using a commercial vibrating sample magnetometer in field-cooled-cooling (FCC) mode. The hysteresis loops were recorded in both field-cooled (FC) and zero-field-cooled (ZFC) modes. In the FC mode, the sample was cooled to 5 K under some magnetic field, and then hysteresis loops were recorded under $\pm 50 \text{ kOe}$ (H_{MAX}), whereas no magnetic field was applied in the ZFC mode. The neutron depolarization experiment was carried out using the polarized neutron spectrometer at Dhruva reactor, Mumbai, India. In this experiment, polarized neutrons ($\lambda = 1.201 \text{ \AA}$) are used to study the domain magnetization of the compound as a function of temperature. Impedance measurements were carried out in the frequency range of 1 Hz–1 MHz by using a PSM1735-NumetriQ impedance analyzer (Newtons4th Ltd., U.K.) over the temperature range of 163–303 K. For impedance measurements, cylindrical pellets of $\text{La}_{1-x}\text{Pr}_x\text{CrO}_3$ compounds with uniformly coated silver paste on both flat sides were used.

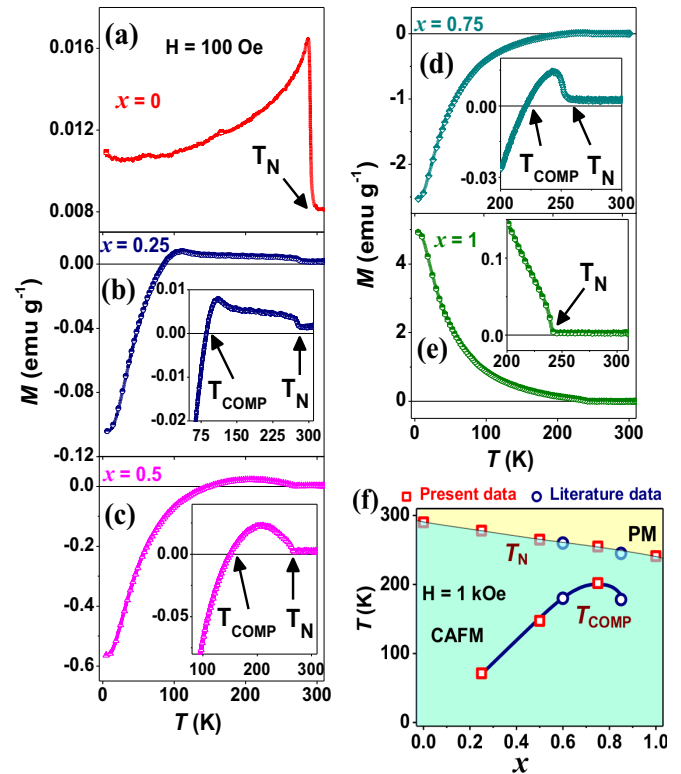


FIG. 1. (a)–(e) $M(T)$ curves measured under magnetic field of $H = 100 \text{ Oe}$ in the FCC mode for $\text{La}_{1-x}\text{Pr}_x\text{CrO}_3$ ($x = 0, 0.25, 0.5, 0.75$, and 1) compounds. The insets show the zoomed-in views of $M(T)$ curves for $x = 0.25, 0.5, 0.75$, and 1 compounds. (f) The magnetic phase diagram of $\text{La}_{1-x}\text{Pr}_x\text{CrO}_3$ compounds depicting the variations of T_N and T_{COMP} with x under $H = 1 \text{ kOe}$. Here CAFM and PM represent the canted antiferromagnetic and paramagnetic states, respectively. The open square symbols (red) represent the present experimental data, whereas the open circular symbols (navy blue) for the $x = 0.6$ and 0.85 compounds have been taken from the literature [14,23]. The solid lines are a guide to the eye.

III. RESULTS

A. X-ray diffraction, and SEM and EDX

Rietveld refined x-ray diffraction patterns at 300 K of all $\text{La}_{1-x}\text{Pr}_x\text{CrO}_3$ ($x = 0, 0.25, 0.5, 0.75$, and 1) compounds are shown in Fig. S1 in the Supplemental Material (SM) [28]. Rietveld analysis shows that all compounds crystallize in the orthorhombic crystal structure with $Pnma$ space group (No. 62). The absence of any extra (unindexed) Bragg peak ratifies the single-phase formation for all the compounds.

The SEM and EDX (Fig. S2 in the SM [28]) measurements have been carried out on Pr^{3+} substituted ($x = 0.25, 0.5$, and 0.75) compounds. The ionic ratios of La^{3+} and Pr^{3+} for these compounds obtained from the EDX are given in Table S1 in the SM [28], and also compared with the values derived from the neutron diffraction (presented later). The results of two measurements are consistent with each other.

B. Magnetic study

1. Dc magnetization

Figures 1(a)–1(e) show the temperature (T) dependence of the dc magnetization (M) for $\text{La}_{1-x}\text{Pr}_x\text{CrO}_3$ ($x = 0, 0.25, 0.5,$

0.75 and 1) compounds measured in the FCC mode under an applied magnetic field (H) of 100 Oe. A magnetic transition is observed in the $x = 0$ compound at a Néel temperature, $T_N \sim 288$ K, which is attributed to the G -type CAFM ordering of Cr^{3+} as reported in the literature [7,29]. The T_N decreases with increase in the Pr^{3+} concentration, as evident from Figs. 1(a)–1(e). Further, the magnetization is found to be positive for the $x = 0$ compound in the whole temperature range below the T_N . An interesting magnetic feature is observed for $x = 0.25, 0.5,$ and 0.75 compounds. These compounds show the NM phenomenon [8], where net dc magnetization becomes negative at $T < T_{\text{COMP}}$. The T_{COMP} values for $x = 0.25, 0.5,$ and 0.75 compounds are $\sim 86, \sim 155,$ and ~ 220 K, respectively, indicating an increase in T_{COMP} with x . Here, it is interesting to note that for this series of compounds, the NM phenomenon appears over a wide Pr^{3+} concentration range ($0.2 \leq x \leq 0.85$) [14], in contrast to $\text{La}_{1-x}\text{Ce}_x\text{CrO}_3$ ($x = 0.9$ and 1) [11] and $\text{Y}_{1-x}\text{Pr}_x\text{CrO}_3$ ($0.05 \leq x \leq 0.2$) [30] compounds which show this phenomenon in a narrow range of magnetic rare-earth ($\text{Ce}^{3+}/\text{Pr}^{3+}$) concentration. For the pure Pr^{3+} compound PrCrO_3 , the NM phenomenon is found to be absent, consistent with the literature reports [14,25,29,31]. We have plotted the magnetic phase diagram of $\text{La}_{1-x}\text{Pr}_x\text{CrO}_3$ compounds showing the variations of T_{COMP} and T_N with x under $H = 1$ kOe [Fig. 1(f)].

2. Exchange bias

Figure 2(a) shows the $M(H)$ hysteresis loops for $x = 0, 0.25, 0.5, 0.75,$ and 1 compounds recorded at 5 K in a cooling field (H_{COOL}) of 5 kOe. The nonsaturating nature of the $M(H)$ loops along with finite coercivity indicates the presence of both ferromagnetic (FM) and antiferromagnetic (AFM) components in these compounds. Further, the hysteresis loops of Pr^{3+} based ($x = 0.25, 0.5, 0.75,$ and 1) compounds are found to be shifted along the horizontal magnetic-field axis. This shift indicates the presence of EB in these compounds; however, zero shift (or zero EB) is found for the $x = 0$ compound. The EB parameter, viz., H_{EB} (horizontal shift), has been estimated using the following equation:

$$H_{\text{EB}} = \frac{H_{C1} + H_{C2}}{2}, \quad (1)$$

where H_{C1} and H_{C2} are the left and right coercivity values, respectively. The variation of H_{EB} with composition (x) is shown in Fig. 2(b). The positive H_{EB} , i.e., hysteresis loop, shifts in the positive H direction, is evident for $x = 0.25, 0.5,$ and 0.75 compounds. As these compounds also exhibit NM [Figs. 1(b)–1(d)], a strong possibility of correlation between NM and EB in the Pr^{3+} substituted compounds is quite eminent. On the other hand, the $x = 1$ compound exhibits negative EB; i.e., the hysteresis loop shifts in the negative H direction. This results in a sign reversal of EB near the $x = 0.75$ compound. Here it is to be noted that, in the literature, the EB with only positive polarity is reported for $x = 0.75$ compound [23] under $H_{\text{COOL}} = 5$ kOe; however, our study has provided the polarity reversal of the EB (involving both positive and negative) in the $\text{La}_{1-x}\text{Pr}_x\text{CrO}_3$ compounds as well as its strong correlation with the NM. We also mention that the sign of EB does not change up to $H_{\text{COOL}} = 50$ kOe in the $x = 0.5$ compound [24].

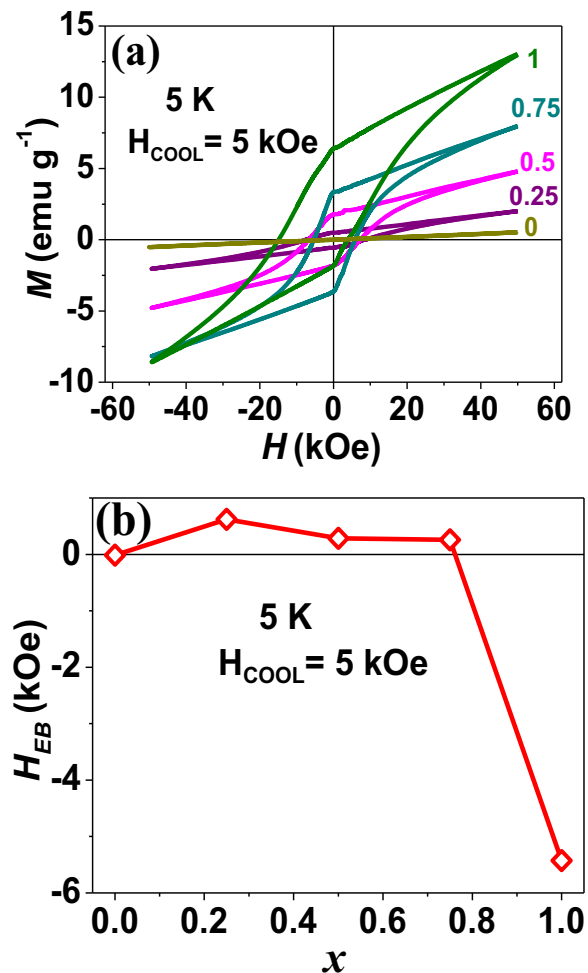


FIG. 2. (a) $M(H)$ hysteresis loops for $x = 0, 0.25, 0.5, 0.75,$ and 1 compounds recorded at 5 K under $H_{\text{COOL}} = 5$ kOe. (b) Variation of the H_{EB} with x .

3. Neutron depolarization

To gain more understanding of the magnetic nature of the $\text{La}_{1-x}\text{Pr}_x\text{CrO}_3$ compounds, we have carried out a temperature-dependent neutron depolarization study. This technique, using polarized neutrons, gives a good estimate of the thermal evolution of magnetization and/or size of magnetic domains over the mesoscopic length scale present in FM/ferrimagnetic/CAFM compounds [32–35]. In particular, in a neutron depolarization experiment involving a NM compound, depolarization of the neutron beam occurs just below the magnetic ordering temperature, where there is a net magnetization of the sample due to finite domain magnetization, followed by a complete recovery of the neutron-beam polarization at the T_{COMP} , which indicates a compensated magnetic state inside the magnetic domain at the T_{COMP} [21,35,36]. Figure 3 depicts temperature dependence of the final polarization (P_f) of the neutron beam transmitted through the $\text{La}_{1-x}\text{Pr}_x\text{CrO}_3$ ($x = 0.25, 0.5, 0.75,$ and 1) compounds. No depolarization is observed for $x = 0$ (not shown) and 0.25 compounds in the whole measured temperature range. On the other hand, $x = 0.5/0.75$ and 1 compounds show finite depolarization of the neutron beam only below 100 and

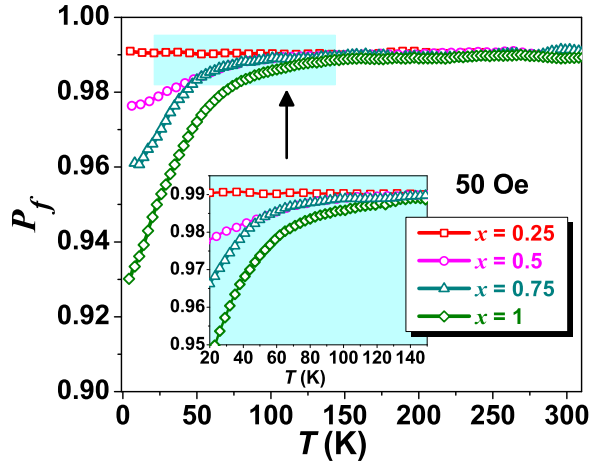


FIG. 3. Temperature dependence of final neutron-beam polarization (P_f) under $H = 50$ Oe for $x = 0.25, 0.5, 0.75,$ and 1 compounds. The inset shows the zoomed-in view of P_f for these compounds.

130 K, respectively (inset of Fig. 3). It may be recalled from Figs. 1(c)–1(e) that dc magnetization of $x = 0.5/0.75$ and 1 compounds becomes significantly large below 100 and 130 K, respectively, to cause a finite depolarization of the neutron beam. For a very small magnetic moment, as is the case for $x = 0$ and 0.25 compounds in the whole measured temperature range, and for $0.5/0.75$ and 1 compounds at $T > 100$ and 130 K, respectively, no depolarization is observed. Consequently, no signatures of T_{COMP} (for $x = 0.25, 0.5,$ and 0.75 compounds) and T_N (for $x = 0, 0.25, 0.5, 0.75,$ and 1 compounds) are found in the present depolarization data. Nevertheless, an increasing neutron-beam depolarization (Fig. 3) with x reveals that domain magnetization is increasing with the Pr (x) substitution. The increasing domain magnetization at low temperatures is an indication of the increasing polarization of the Pr^{3+} moments under the internal field of ordered Cr^{3+} moments, and is consistent with the increasing dc magnetization with x (Fig. 1) below the T_{COMP} . Our temperature-dependent neutron diffraction results (presented later) for Pr^{3+} substituted compounds infer no sign of spontaneous magnetic ordering of Pr^{3+} moments due to Pr^{3+} - Pr^{3+} exchange interaction.

Further, from the observed depolarization data, we have estimated the average domain size using the following equation [32–34]:

$$P_f = P_i \exp \left[-\alpha \left(\frac{d}{\delta} \right) (\Phi_\delta)^2 \right], \quad (2)$$

where P_i/P_f is the initial/final neutron-beam polarization, α ($\sim 1/3$) is a dimensionless parameter, d (~ 2.53 mm) is the effective thickness of the sample, and $\Phi_\delta = (4.63 \times 10^{-10} \text{ G}^{-1} \text{ \AA}^{-2}) \lambda B \delta$ is the precession angle for a neutron of wavelength λ (1.201 \AA) traveling a distance δ (average domain size) inside a domain of magnetization, B ($=4\pi M_s \rho$). Here, M_s and ρ are the saturation magnetization and density of the compounds in emu g^{-1} and g cm^{-3} , respectively. Domain magnetization B at 5 K for $x = 0.5, 0.75,$ and 1 compounds is estimated using corresponding M_s and ρ values of these compounds. The M_s values have been estimated from ZFC

$M(H)$ hysteresis loops at 5 K (not shown), after subtracting the AFM contribution. Using these values in Eq. (2), δ of the order of ~ 10 μm at 5 K for $x = 0.5$ – 1 compounds has been estimated. The μm sized FM domains reveal that the origin of the FM component in the present compounds is due to the spin canting of the AFM ground state, not due to any phase separation between FM and AFM phases, where smaller FM domain size is expected [37].

In summary, Pr^{3+} substitution has resulted in significant changes in the magnetic properties of the present $\text{La}_{1-x}\text{Pr}_x\text{CrO}_3$ compounds. To investigate the corresponding changes in electrical properties of these compounds, we have employed impedance spectroscopy. The results of this technique are discussed in the next section.

C. Electrical study

1. Impedance spectroscopy

Complex impedance spectroscopy (CIS) is a well-known nondestructive technique to study the electrical properties of a compound. Using CIS, one can separately determine the contributions of grain interior, grain boundary, and sample-electrode interface to the conduction of charge carriers [38]. We have measured the complex impedance (Z^*) of the $\text{La}_{1-x}\text{Pr}_x\text{CrO}_3$ ($x = 0, 0.25, 0.5, 0.75,$ and 1) compounds using the CIS technique as a function of frequency (1 Hz– 1 MHz) and temperature (163 – 303 K) to investigate the electrical properties.

Figures 4(a) and 4(b) show the frequency dependence of the real (Z') and imaginary (Z'') parts of $Z^* = Z' + jZ''$ at selected temperatures. It is found that the magnitude of Z' at a given frequency decreases with increase in temperature, suggesting the increase in ac conductivity (presented later) of $\text{La}_{1-x}\text{Pr}_x\text{CrO}_3$ compounds. On the other hand, Z'' vs frequency curves exhibit a peak at a characteristic frequency (f_{max}) over a whole temperature range. With increase in temperature, the peak shifts toward the high frequency side indicating the temperature-dependent relaxation [39] in $\text{La}_{1-x}\text{Pr}_x\text{CrO}_3$ compounds. This relaxation can be analyzed by the Arrhenius law, $f_{\text{max}} = f_0 \exp(-E_a/k_B T)$, where f_0 is the preexponential factor, E_a is the activation energy, and k_B is the Boltzmann constant. The E_a values, determined from the Arrhenius fitting of $\ln(f)$ vs $1000/T$ plots [Fig. 4(c)], are 0.27 (1), 0.28 (1), 0.29 (1), 0.24 (2), and 0.28 (1) eV for $x = 0, 0.25, 0.5, 0.75,$ and 1 compounds, respectively. These E_a values are in good agreement with values reported for $R\text{CrO}_3$ compounds [25,40,41].

Figure 5(a) shows the Nyquist or Cole-Cole plots [42] ($-Z''$ vs Z' curves) for a few temperatures to estimate the contributions of grain, grain boundary, and electrode to the impedance. The presence of a single semicircle in the Nyquist plot for all compounds indicates negligible grain boundary and electrode contributions to the impedance. Hence, the whole contribution comes from the grain interior [43] of the $\text{La}_{1-x}\text{Pr}_x\text{CrO}_3$ compounds. The observed single and depressed semicircle with its center lying below the real axis in the Nyquist plots indicates non-Debye-type relaxation [44]. Similar behavior of the Cole-Cole plots was reported earlier for other $R\text{CrO}_3$ compounds [40,43]. For each compound, we have modeled the observed depressed semicircle with a parallel combination of

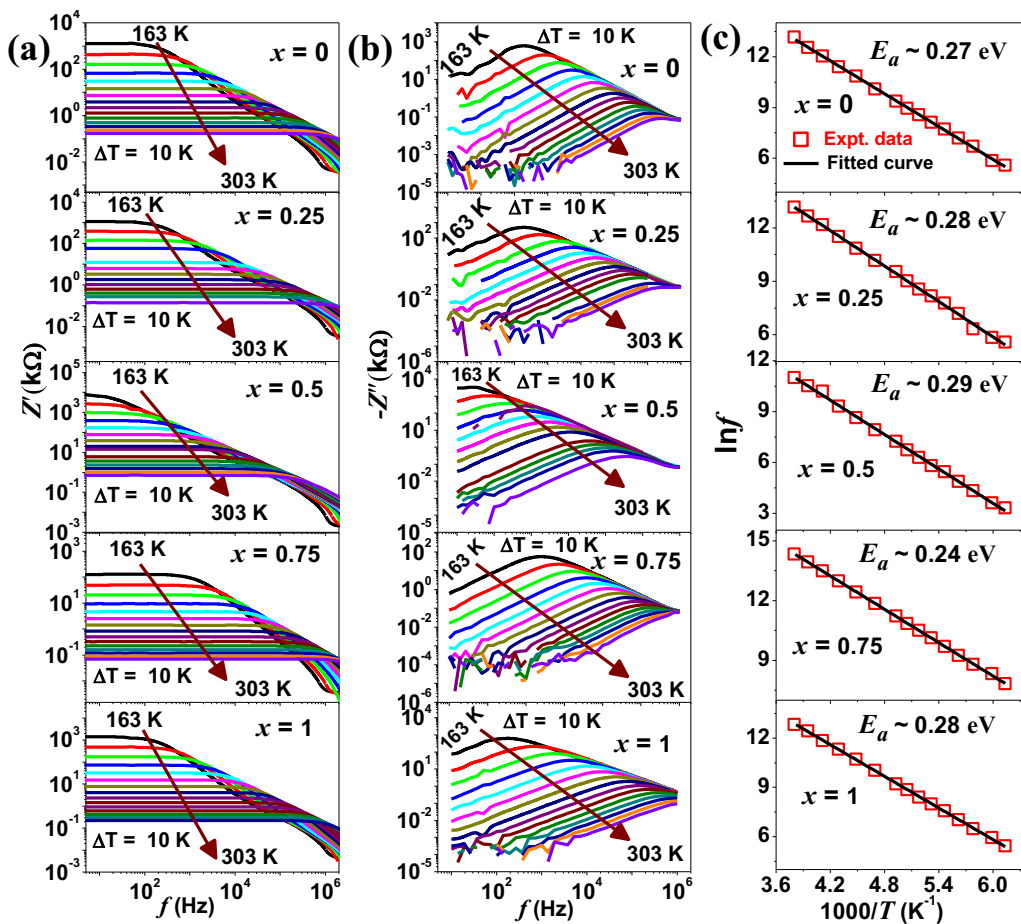


FIG. 4. Frequency dependence of the (a) real (Z') and (b) imaginary ($-Z''$) parts of complex impedance (Z^*) at selected temperatures. (c) Variation of $\ln(f)$ vs $1000/T$ (red square symbols) and the black lines show the fitted curves by the Arrhenius law.

resistance (R_g) and constant phase element (CPE) [Fig. 5(b)]. The impedance of the CPE is given by $Z_{\text{CPE}} = \frac{1}{(j\omega)^n \text{CPE}}$, where n ($0 \leq n \leq 1$) measures the depression of the semicircle. The value of $n = 1$ corresponds to Debye-type relaxation, while $n > 1$ indicates non-Debye-type relaxation. The $-Z''$ vs Z' curves have been fitted with an equivalent circuit shown in Fig. 5(b) using the EIS SPECTRUM ANALYSER software [45] and values of n , R_g , and CPE have been determined. Figure 5(c) shows the variations of n and CPE with Pr^{3+} concentration (x) at 203 K. It is noteworthy here that the value of n is less than 1 for all the compounds indicating a non-Debye-type relaxation. The CPE value is of the order of a nanofarad (nF), which could be attributed to the grain interior or bulk contribution [38,46]. Using the R_g values, we have estimated the dc conductivity using the relation $\sigma_{\text{dc}} = tR_g/A$, where t and A are the thickness and area of the pellet, respectively. The inverse temperature dependence of dc conductivity follows the Arrhenius equation $\sigma_{\text{dc}} = \sigma_0 \exp(-E_a/k_B T)$, as shown in Fig. 5(d), where σ_0 is the preexponential factor, E_a is the activation energy required for conduction, and k_B is the Boltzmann constant. The derived values of E_a from the above equation are ~ 0.27 (1), 0.28 (1), 0.29 (1), 0.24 (2), and 0.27 eV (1), respectively, for $x = 0, 0.25, 0.5, 0.75$, and 1 compounds. These values of E_a are close to the values obtained from the Arrhenius fitting of characteristic peak frequency (f_{max}) [Fig. 4(c)]. Moreover, these

values are in good agreement with literature reported values for related compounds [47,48]. Here, it is also noted that E_a is the minimum for the $x = 0.75$ compound, which coincides with the maximum T_{COMP} [Fig. 1(f)] for the same compound. Conduction mechanism/properties are further studied by analyzing the ac conductivity as follows.

2. Ac conductivity

Frequency dependence of ac conductivity (σ_{ac}) has been calculated from the complex impedance (Z^*) using the following equation:

$$\sigma_{\text{ac}} = \frac{t}{A} \frac{Z'^2}{Z'^2 + Z''^2}. \quad (3)$$

Figure 6(a) shows the frequency dependence of σ_{ac} for $\text{La}_{1-x}\text{Pr}_x\text{CrO}_3$ ($x = 0, 0.25, 0.5, 0.75$, and 1) compounds at various temperatures with an interval of 20 K. It is evident that at a given frequency, σ_{ac} increases with increase in temperature, reflecting the semiconducting nature of the compounds [40]. Also, with increasing temperature, the dc plateau (frequency-independent conductivity) extends up to higher frequency values. Figure 6(b) shows the σ_{ac} as a function of x for some selected temperatures at a frequency of 1 kHz. At any temperature (163–303 K), σ_{ac} first decreases up to $x = 0.5$, then starts to increase, shows maximum value

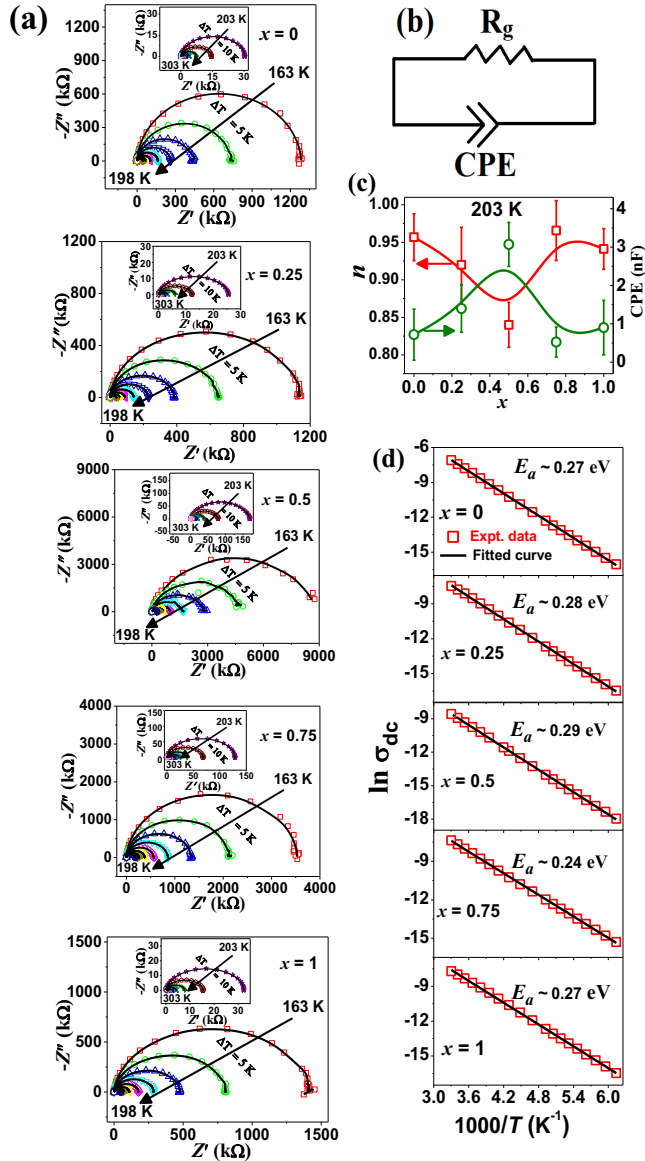


FIG. 5. (a) Cole-Cole plots of the impedance data at some selected temperatures for the $\text{La}_{1-x}\text{Pr}_x\text{CrO}_3$ ($x = 0, 0.25, 0.5, 0.75,$ and 1) compounds. (b) Equivalent circuit that is considered to fit the Cole-Cole plots. (c) Variations of n and CPE with x at 203 K. (d) The Arrhenius fitting (black lines) of $\ln \sigma_{\text{dc}}$ vs $1000/T$ curves (red square symbols) for all compounds.

at $x = 0.75$, and thereafter it decreases again. This maximum in σ_{ac} for intermediate compound ($x = 0.75$) is in agreement with the $\text{GdCo}_{1-x}\text{Cr}_x\text{O}_3$ ($x = 0, 0.33, 0.5, 0.67,$ and 1) compounds [49], where maximum σ_{ac} was reported for $x = 0.67$. In contrast, the monotonic decreasing σ_{ac} with x was reported for $\text{La}_{1-x}\text{Pr}_x\text{MnO}_3$ ($0 \leq x \leq 1$) compounds [50] which might be due to the presence of the Jahn-Teller (Mn^{3+}) ion in $\text{La}_{1-x}\text{Pr}_x\text{MnO}_3$ compounds.

To get insight about the conduction mechanism, the frequency dependence of σ_{ac} was analyzed by the power law given by Jonscher [51] as

$$\sigma_{\text{ac}} = \sigma_{\text{dc}} + A\omega^s, \quad (4)$$

where σ_{dc} is the dc or frequency-independent conductivity; ω ($=2\pi f$) is the angular frequency; coefficient A and frequency exponent s (value lies between 0 and 1) are the temperature and material-dependent-intrinsic constants. The s represents the degree of interaction of charge carriers with the environment surrounding them, while A represents the strength of polarizability. The σ_{ac} curves are fitted with Eq. (4) and values of σ_{dc} , s , and A are determined.

Variation of exponent s with temperature provides insight into the conduction mechanism [52]. Figure 6(c) shows the variation of s as a function of temperature for all the compounds. For LaCrO_3 ($x = 0$ compound), exponent s first decreases with increasing temperature, reaches a minimum value and then increases with further increasing temperature. Similar behavior of s for LaCrO_3 compound is reported in the literature [43]. Such observed behavior of s corresponds to the overlapping large polaron tunneling (OLPT) mechanism for conduction as reported by Coşkun *et al.* [43]. The same mechanism also explains the conduction for $x = 0.25$ and 1 compounds. Interestingly, the temperature dependence of s shows different behavior for intermediate compounds with $x = 0.5$ and 0.75 . For $x = 0.5$, exponent s first increases with increase in temperature, and then it follows the OLPT mechanism above ~ 200 K. Initial increase of exponent s for $x = 0.5$ compound indicates a nonoverlapping small polaron tunneling (NSPT) [53]-type conduction mechanism, whereas, for $x = 0.75$, the NSPT-type conduction mechanism is evident over the whole measured temperature range.

In brief, the $x = 0.75$ compound shows a maximum σ_{ac} with minimum activation energy. In order to get a microscopic understanding of peculiar magnetic and electrical properties in $\text{La}_{1-x}\text{Pr}_x\text{CrO}_3$ compounds, the neutron diffraction technique has been employed, which will be discussed in the next section.

D. Neutron diffraction

Figure 7(a) shows the Rietveld refined ND patterns at 300 K for all the studied compounds of the series. Recorded patterns show that the intensities of some of the Bragg peaks, viz., $\{(101) (020)\}$, (200) , (201) , (112) , (004) , and $\{(251) (233)\}$ [shown by shaded area in Fig. 7(a)] monotonically change, involving increasing/decreasing intensities of $\{(101) (020)\}$, (201) , (112) , $\{(251) (233)\}/(200)$, (004) , with increasing Pr^{3+} substitution. In addition, the Bragg peaks are shifted toward higher Q values with increasing Pr^{3+} concentration in $\text{La}_{1-x}\text{Pr}_x\text{CrO}_3$ [Fig. 7(b)], indicating the contraction of the lattice parameters and unit-cell volume. This can be attributed to the smaller ionic size of Pr^{3+} (1.13 \AA) as compared to that of the La^{3+} (1.17 \AA) ion, which reduces the average A -site ionic radius and hence contraction of the unit cell. The derived values of the lattice parameters a , b , and c for end compounds LaCrO_3 ($x = 0$) and PrCrO_3 ($x = 1$) are 5.482 (1) \AA , 7.774 (2) \AA , and 5.516 (1) \AA ; and 5.475 (2) \AA , 7.703 (2) \AA , and 5.451 (1) \AA , respectively, which are in good agreement with the literature reported values [29,54,55]. Lattice parameter b is found to be larger than both a and c for all compounds and it decreases monotonically with increasing x [Fig. 7(c)]. Further, the lattice parameter c ($>a$ for $x = 0$) decreases more rapidly with Pr^{3+} substitution as compared to the lattice parameter

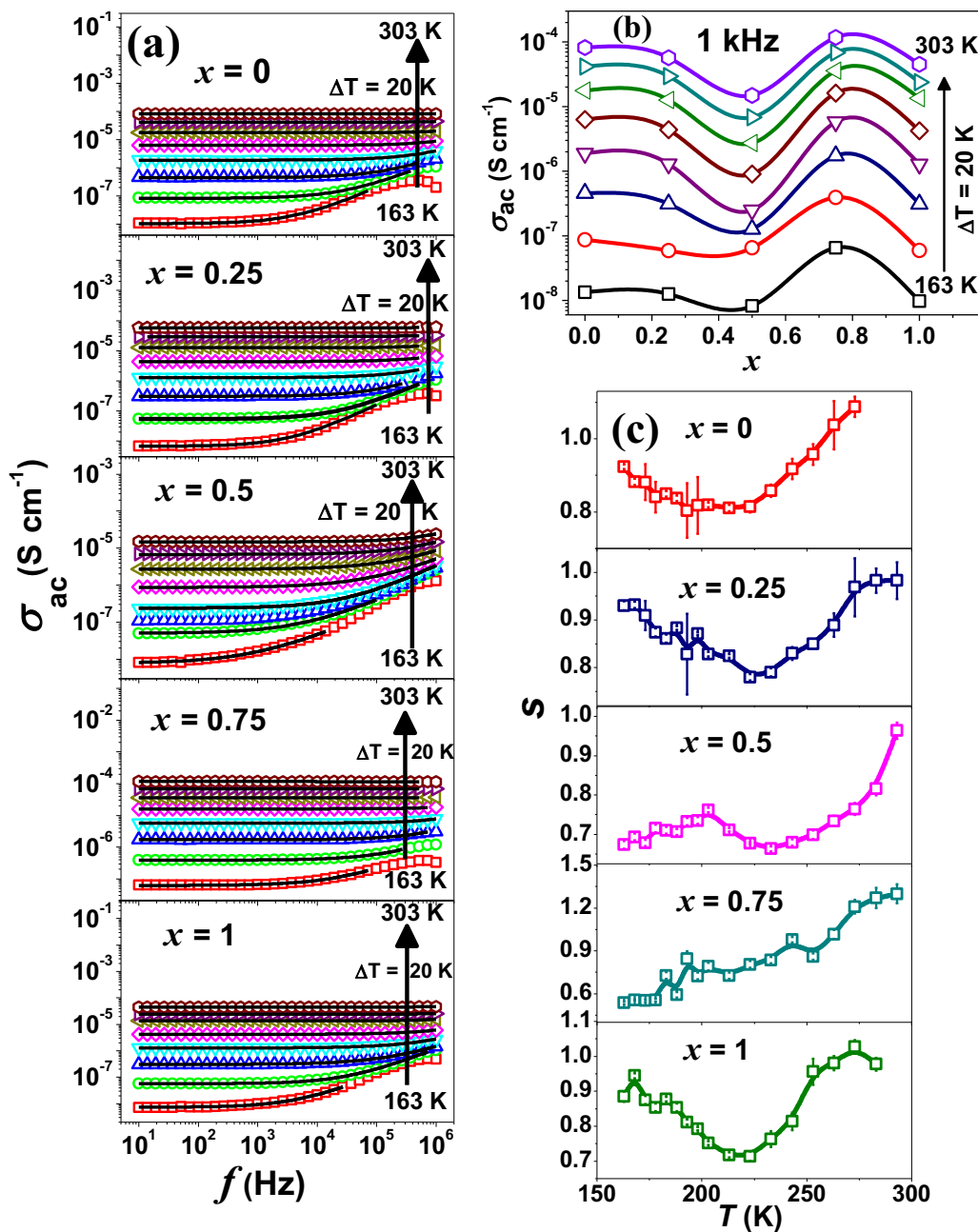


FIG. 6. (a) Frequency dependence of ac conductivity (σ_{ac}) of $\text{La}_{1-x}\text{Pr}_x\text{CrO}_3$ ($x = 0, 0.25, 0.5, 0.75$, and 1) compounds over a temperature range of 163–303 K with an interval of 20 K. Here experimental data are shown by symbols, and the solid black line shows a fit to experimental data as per Jonscher's law. (b) Variation of σ_{ac} with x over a temperature range of 163–303 K with an interval of 20 K at a frequency of 1 kHz. (c) Variation of the s with temperature for all the compounds.

a , and as a result, c becomes smaller than a for $x \gtrsim 0.75$. This changes the lattice parameters' relation from $c > a$ to $c < a$ around $x = 0.75$ [Fig. 7(c)], which is attributed to the equatorial bond lengths' (lying in the ac plane) variation with x (Fig. S3 in the SM [28]). Interestingly, this crossover persists at low temperatures also (Fig. S4 in the SM [28]), as evident from the Rietveld refinement of low temperature ND data (to be discussed later). Owing to the almost similar values of the lattice parameters a and c for $x = 0.75$, i.e., high symmetry crystal structure [49], charge carriers (polaron) can tunnel in more than one direction, leading to the highest conductivity

for this compound, which is further consistent with its minimum E_a (required for conduction). Further, estimated atomic positions, bond angles, bond distances, and reliability factors are listed in Table S2 in the SM [28]. The average bond angle (θ), estimated using θ_1 and θ_2 , is found to decrease monotonically with x (Fig. S3 in the SM [28]).

To get the orientations of magnetic moments in the Pr^{3+} substituted compounds, temperature-dependent neutron diffraction is carried out. Figure 8(a) depicts the Rietveld refined ND patterns of Pr^{3+} substituted ($x = 0.25, 0.5, 0.75$, and 1) compounds at 5 K. From comparison of the ND pat-

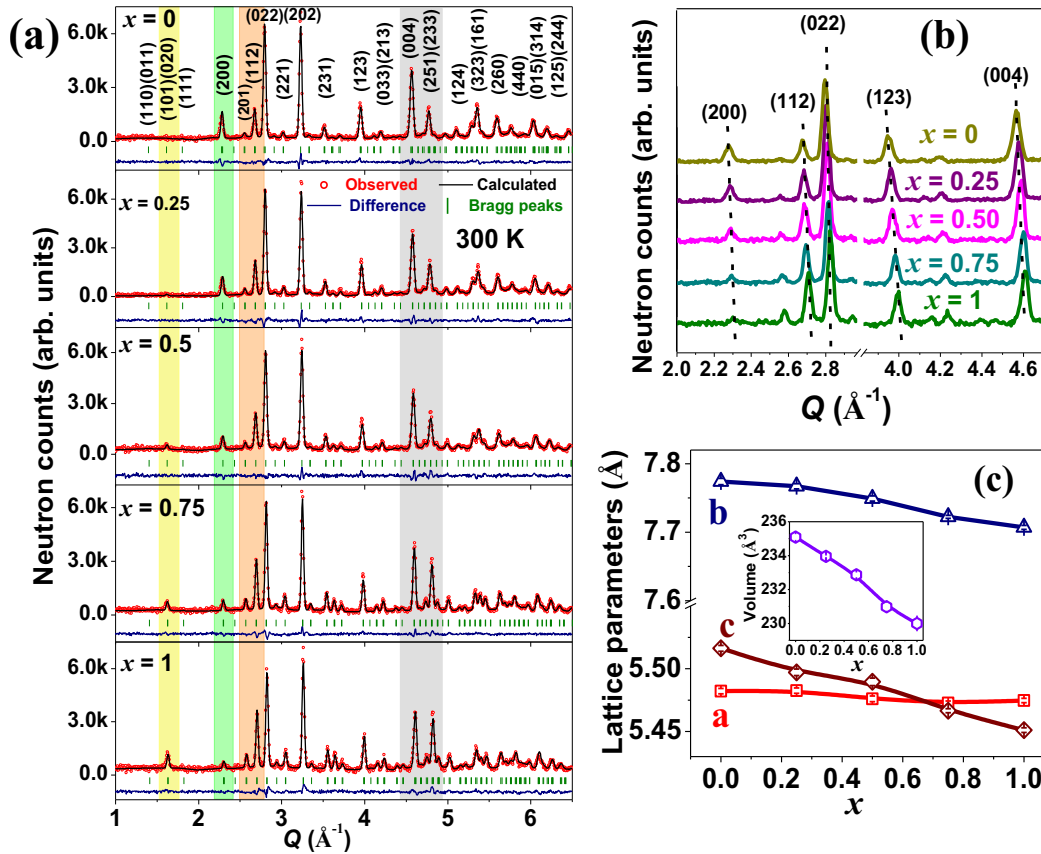


FIG. 7. (a) Rietveld refined ND patterns of the $\text{La}_{1-x}\text{Pr}_x\text{CrO}_3$ ($x = 0, 0.25, 0.5, 0.75,$ and 1) compounds at 300 K . (b) Selected portion of the ND patterns highlighting the shifting of (200) , (112) , (022) , (123) , and (004) Bragg peaks toward higher Q with increasing x . (c) Variations of the lattice parameters and unit-cell volume (inset) with x .

terns at 300 K [Fig. 7(a)] and 5 K [Fig. 8(a)], it is found that the $\{(110)(011)\}$ Bragg peak positioned at $Q = 1.40\text{ \AA}^{-1}$ gain in intensity at 5 K due to magnetic contribution. Thus, in addition to the nuclear phase, a magnetic phase has been added in the Rietveld refinement to fit this magnetic contribution. Here we mention that the nuclear phase is of the same symmetry ($Pnma$) as used for the Rietveld refinement of ND at 300 K . Rietveld refinement of the ND data (at 5 K) reveals that Cr^{3+} magnetically orders into $\Gamma_2(G_yF_z)$ spin configuration with the finite G_y component in all compounds. Here G_y means the AFM component of the Cr^{3+} moment along the $y(b)$ axis, and F_z is the FM component along the $z(c)$ axis, which arises due to the spin canting of Cr^{3+} . It may be noted that the same (nuclear + magnetic) model gives good agreement between the observed and calculated ND data in the $5\text{ K} < T \leq T_N$ temperature range for $x = 0.25$ to 1 compounds, indicating no structural phase transition in these compounds at $T \leq T_N$. Moreover, it also reveals that there is no spin-orientation-like transition in any of these compounds. Figure 8(b) shows the variation of the AFM component (G_y) of the Cr^{3+} moment with temperature for Pr^{3+} substituted ($x = 0.25, 0.5, 0.75,$ and 1) compounds, following the Brillouin-function-type temperature dependence. Further, it is known that the FM (F_z) component of the Cr^{3+} is generally very small ($\sim 10^{-2}$ – $10^{-5}\mu_B$) in $R\text{CrO}_3$ compounds [56]; thus it is not possible to get this small component using the present ND study. However, the FM contribution is evident

from the dc magnetization data (Figs. 1 and 2). On the other hand, no signature of spontaneous ordering of Pr^{3+} (T_N^{Pr}) due to Pr^{3+} - Pr^{3+} exchange interaction is found in all Pr^{3+} substituted compounds down to 5 K , which is consistent with the literature reports [14,24,25]. The magnetic structure of the compounds consisting of only the G_y AFM component is depicted in the inset of Fig. 8(b). Further, the estimated lattice parameters for $x = 0.25$ to 1.0 compounds at various temperatures from the Rietveld refinement of the ND patterns are shown in Fig. S4 in the SM [28].

IV. DISCUSSION

Experimental results of the present study reveal that the structural, magnetic, and electrical properties of $\text{La}_{1-x}\text{Pr}_x\text{CrO}_3$ ($x = 0, 0.25, 0.5, 0.75,$ and 1) compounds vary significantly with increasing Pr^{3+} substitution. It is evident from the dc magnetization study that compounds with Pr^{3+} concentration in the range of $0.25 \leq x \leq 0.75$ show the NM phenomenon with maximum T_{COMP} for the $x = 0.75$ compound [Fig. 1(f)]. FC $M(H)$ hysteresis loops reveal the presence of the FM contribution in $\text{La}_{1-x}\text{Pr}_x\text{CrO}_3$ compounds due to Cr^{3+} spin canting [Fig. 2(a)]. Further, the ND study has revealed that, in all compounds, Cr^{3+} orders into the $\Gamma_2(G_yF_z)$ spin configuration, and no signature of spontaneous ordering of Pr^{3+} (T_N^{Pr}) due to Pr^{3+} - Pr^{3+} exchange interaction is found down to 5 K . However, the CAFM ordering of Cr^{3+} creates an internal

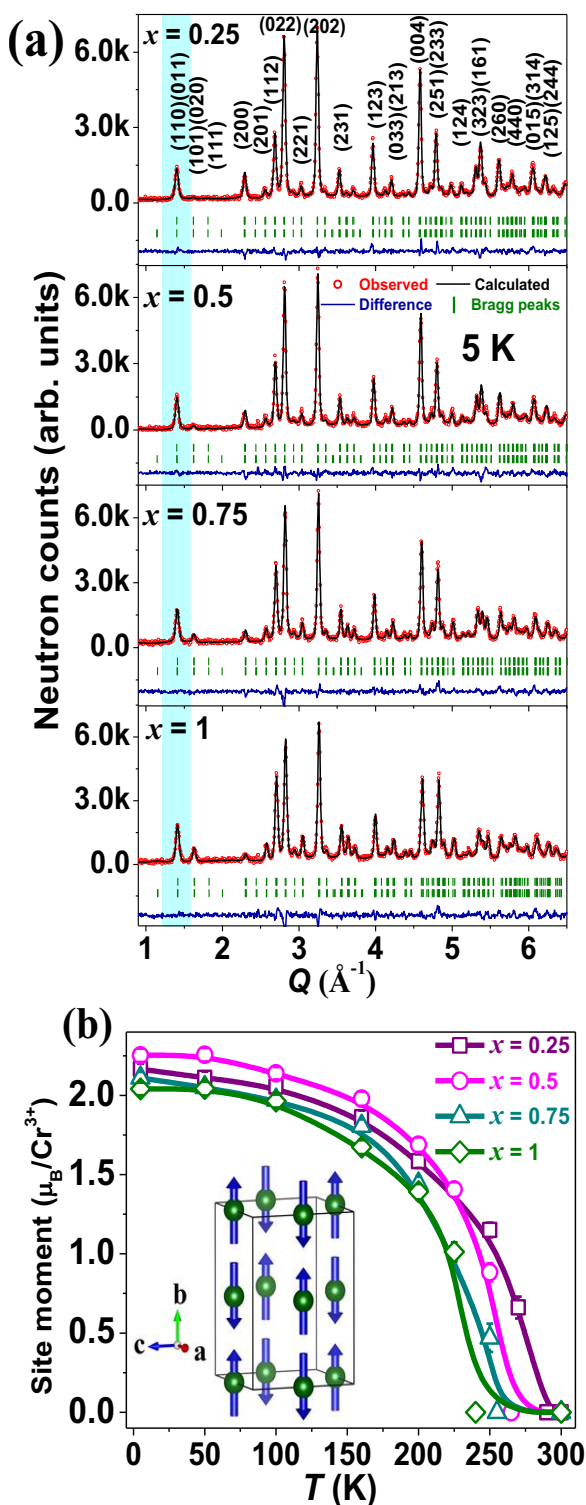


FIG. 8. (a) The Rietveld refined ND patterns for $x = 0.25, 0.5, 0.75,$ and 1 compound at 5 K. Here, the experimental data are shown by the open symbols (red color), and the solid black line shows the calculated patterns. The difference of these two data is shown at the bottom by the navy blue line. The upper and lower vertical lines (olive color) represent the positions of nuclear and magnetic Bragg peaks, respectively. (b) Temperature variation of AFM component of Cr^{3+} moment for $x = 0.25$ – 1 compounds. The solid lines are a guide to the eye. The inset shows the magnetic structure of the compounds involving G_y -type AFM spin configuration of Cr^{3+} ions.

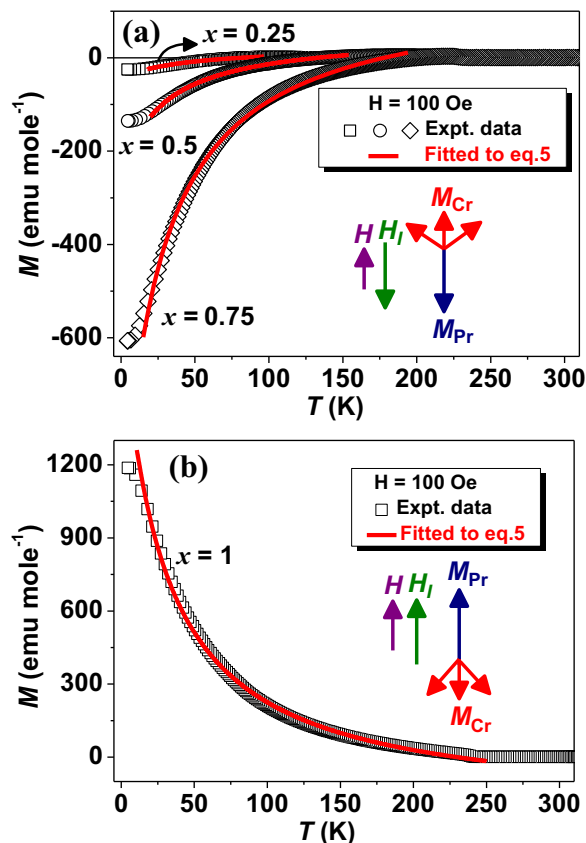


FIG. 9. M vs T data under $H = 100$ Oe (open symbols) and their fitting (solid red line) using Cooke's model [57] for (a) $x = 0.25, 0.5, 0.75,$ and (b) $x = 1$ compounds. The schematics of the spin arrangement of the M_{Cr} (red) and M_{Pr} (navy blue) moments under the influence of H (purple) and H_I (olive) for all of these compounds are shown in their corresponding insets.

magnetic field (H_I) that causes polarization of the Pr^{3+} (M_{Pr}) moment. It is possible to explain the observed NM and variation of T_{COMP} with x by considering temperature dependences of the M_{Cr} (FM component of Cr^{3+}) and M_{Pr} moments. We have used the model proposed by Cooke *et al.* [57] which involves the fitting of the dc magnetization vs temperature data. According to this model, the magnetization behavior for $T \leq T_{\text{COMP}}$ is governed by the following equation:

$$M = M_{\text{Cr}} + \frac{C(H + H_I)}{(T + \theta)}. \quad (5)$$

Here M_{Cr} is the FM component of the Cr^{3+} moment, H and H_I are the applied and internal magnetic fields, respectively, and θ is the Curie-Weiss constant. Furthermore, $C = xC_{\text{Pr}}$ is the Curie constant, which depends on the x and experimental Curie constant of Pr^{3+} (C_{Pr}). The M vs T data for $x = 0.25, 0.5,$ and 0.75 compounds under $H = 100$ Oe have been fitted with Eq. (5) [Fig. 9(a)], and corresponding parameters, viz., M_{Cr} and H_I , have been derived (Table I). For comparison, literature values of M_{Cr} and H_I are also given. The derived M_{Cr} values are positive, indicating its alignment in the direction of H , whereas negative values of H_I infer that the internal field polarizes M_{Pr} opposite to H as well as M_{Cr} . The dominance of M_{Pr} over M_{Cr} (aligned along H) below T_{COMP} results in the

TABLE I. Parameters obtained from the fitting of the present dc magnetization data under $H = 100$ Oe using Cooke's model and its comparison with the literature reported values [14,23,31].

x	M_{Cr} (emu mole ⁻¹)		H_I (kOe)	
	Present	Literature	Present	Literature
0.25	24	— ^a	-7.8	— ^a
0.5	51	40	-10.1	-8.5
0.75	150	— ^a	-25	-16
1	-220	-200	35	30

^aNot reported.

NM in $La_{1-x}Pr_xCrO_3$ ($x = 0.25, 0.5,$ and 0.75) compounds. The spin arrangements for these compounds involving the AFM coupling between the Cr^{3+} and Pr^{3+} moments are shown in the inset of Fig. 9(a). Further, it is found that the value of $|H_I|$ increases with x (Table I), indicating the dominance of M_{Pr} over M_{Cr} at relatively higher temperatures with increasing x . This explains increasing T_{COMP} with increasing x [Fig. 1(f)]. It is known from the literature that $|H_I| \sim 2.8$ to 3 kOe for the $x = 0.85$ compound [23]. This sudden decrease in $|H_I|$ from ~ 25 kOe for $x = 0.75$ to ~ 3 kOe for $x = 0.85$ clearly explains the decrease in T_{COMP} for $x = 0.85$ [Fig. 1(f)]. Further, the dc magnetization data of the $x = 1$ compound is also fitted with Eq. (5) [Fig. 9(b)] in almost the whole temperature range below T_N with $M_{Cr} \sim -220$ emu mole⁻¹ and $H_I \sim 35$ kOe. These values are quite close to literature reported values [31] for $PrCrO_3$ (Table I). The respective signs of these parameters indicate that for the $x = 1$ compound, positive magnetization of $PrCrO_3$ is dominated by M_{Pr} polarized along H , and M_{Cr} is opposite to both. The schematic of the spin arrangement of these moments preserving the AFM coupling between them is depicted in the inset of Fig. 9(b). Here we add that the $LaCrO_3$ ($x = 0$) compound has only one magnetic sublattice, i.e., Cr^{3+} ; thus it does not encounter any intersublattice magnetic interaction, and hence the NM phenomenon is absent in this compound.

In addition to the NM phenomenon for $0.25 \leq x \leq 0.75$ compounds, another unique phenomenon, viz., EB, is also observed for all Pr substituted compounds including $x = 1$. It is known that EB arises as a result of the coupling between two or more magnetic sublattices with an interfacial coupling [10]. That is why the present $x = 0$ compound with a single magnetic sublattice does not exhibit this phenomenon [Fig. 2(b)]. For $x = 0.25$ to 0.75 compounds with two (i.e., M_{Cr} and M_{Pr}) magnetic sublattices, the NM state is favorable below T_{COMP} (Fig. 1) under a positive magnetic field. This leads to an easy switching of the magnetization sign while decreasing the field from $+H_{MAX}$ in a hysteresis loop measurement. This makes H_{C1} smaller. On the other hand, a higher magnetic field is required to make magnetization positive while traversing from $-H_{MAX}$ to $+H_{MAX}$, because the positive magnetization state is energetically unfavorable in the NM state. This leads to the higher H_{C2} and consequently, a positive H_{EB} is observed for these compounds. This mechanism also explains the negative H_{EB} for the $x = 1$ compound [Fig. 2(b)], where the positive magnetization state is energetically favorable leading to the higher H_{C1} and lower H_{C2} .

In contrast to the T_{COMP} , T_N has shown a decrease with increasing x in the present $La_{1-x}Pr_xCrO_3$ compounds [Fig. 1(f)]. The decrease in T_N with increasing x is explained by the decrease in the indirect overlapping of Cr^{3+} orbitals leading to the decrease in superexchange interaction, which is clearly anticipated from the decreasing $\langle Cr^{3+}-O^{2-}-Cr^{3+} \rangle$ bond angle (Fig. S3 in the SM [28]). To generalize this picture, we have plotted the variation of the T_N with A -site ionic radii (Fig. S5 in the SM [28]) of $R_{1-x}R'_xCrO_3$ compounds [11,12,17,30,40,54,58–70], where R and R' are the rare earths (La to Lu, Y) having different ionic radii. It is interesting to note that T_N decreases linearly with the decrease in average ionic radii of the A site for all the $R_{1-x}R'_xCrO_3$ reported compounds. Interestingly, a similar variation of T_N with A -site ionic radii has been observed for isostructural manganites, $R_{1-x}R'_xMnO_3$ [50] and orthoferrites, $R_{1-x}R'_xFeO_3$ [71].

V. SUMMARY AND CONCLUSIONS

The systematic and comprehensive study of structural, magnetic, and electrical properties of Pr^{3+} substituted $La_{1-x}Pr_xCrO_3$ ($x = 0, 0.25, 0.5, 0.75,$ and 1) compounds has been done by x-ray and neutron diffraction, SEM and EDX, dc magnetization, neutron depolarization, and complex impedance spectroscopy. The dc magnetization study has revealed the presence of an unusual negative magnetization (NM) phenomenon in $x = 0.25, 0.5,$ and 0.75 compounds with increasing compensation temperature (T_{COMP}) with x . The systematic increase in T_{COMP} with x is explained within the framework of Cooke's model involving competition between polarized Pr^{3+} moments under increasing internal field and canted Cr^{3+} moments. Further, positive exchange bias (EB) is evident for these compounds involving NM, indicating a correlation between NM and a positive sign of EB in the Pr^{3+} substituted compounds. On the other hand, negative EB is found for $x = 1$ compound involving no NM. Moreover, dc magnetization is also found to be increasing with increasing Pr^{3+} concentration, which is consistent with the increasing neutron-beam depolarization with x . In contrast to the increasing T_{COMP} , magnetic ordering temperature T_N decreases monotonically from ~ 288 K ($x = 0$) to 240 K ($x = 1$) which is attributed to the decreasing average bond angle $\langle Cr^{3+}-O^{2-}-Cr^{3+} \rangle$ with increasing x , as estimated from neutron diffraction. Interestingly, our study has shown that such linear decreasing behavior of T_N with average A -site ionic radii is universal and holds for all other rare-earth-substituted orthochromite compounds also. Further, maximum ac conductivity (with minimum activation energy required for conduction) for the $x = 0.75$ compound is explained in terms of the crossover of lattice parameters from $a < c$ to $a > c$ across $x \sim 0.75$. Moreover, the conduction mechanism also shows peculiar change as a function of x in $La_{1-x}Pr_xCrO_3$ compounds. The overlapping large polaron tunneling (OLPT) mechanism explains the conduction for $x = 0, 0.25,$ and 1 compounds, while nonoverlapping small polaron tunneling (NSPT) explains conduction for $x = 0.75$. A mixture of both OLPT and NSPT mechanisms accounts for conduction in $x = 0.5$. Thus, our study has revealed an understanding of unique phenomena of NM and EB, and the variation of electrical properties in $La_{1-x}Pr_xCrO_3$ compounds.

ACKNOWLEDGMENT

Deepak acknowledges the help provided by P. U. Sastry and V. B. Jayakrishnan for x-ray diffraction measurements.

-
- [1] T. Arakawa, S. Tsuchi-ya, and J. Shiokawa, *Mater. Res. Bull.* **16**, 97 (1981).
- [2] Z. Shao, W. Zhou, and Z. Zhu, *Prog. Mater. Sci.* **57**, 804 (2012).
- [3] M. Siemons, A. Leifert, and U. Simon, *Adv. Funct. Mater.* **17**, 2189 (2007).
- [4] S. M. Khetre, A. U. Chopade, C. J. Khilare, H. V. Jadhav, P. N. Jagadale, and S. R. Bamane, *J. Mater. Sci. Mater. Electron.* **24**, 4361 (2013).
- [5] G. V. S. Rao, B. M. Wanklyn, and C. N. R. Rao, in *Solid State Chemistry* (World Scientific, Singapore, 1995), p. 365.
- [6] J. Sfeir, *J. Power Sources* **118**, 276 (2003).
- [7] K. D. Singh, F. Singh, R. J. Choudhary, and R. Kumar, *Appl. Phys. A* **126**, 148 (2020).
- [8] A. Kumar and S. M. Yusuf, *Phys. Rep.* **556**, 1 (2015).
- [9] A. Kumar, S. M. Yusuf, and C. Ritter, *Phys. Rev. B* **96**, 014427 (2017).
- [10] P. K. Manna and S. M. Yusuf, *Phys. Rep.* **535**, 61 (2014).
- [11] R. Shukla, J. Manjanna, A. K. Bera, S. M. Yusuf, and A. K. Tyagi, *Inorg. Chem.* **48**, 11691 (2009).
- [12] N. Sharma, B. K. Srivastava, A. Krishnamurthy, and A. K. Nigam, *Solid State Sci.* **12**, 1464 (2010).
- [13] V. A. Khomchenko, I. O. Troyanchuk, R. Szymczak, and H. Szymczak, *J. Mater. Sci.* **43**, 5662 (2008).
- [14] K. Yoshii, A. Nakamura, Y. Ishii, and Y. Morii, *J. Solid State Chem.* **162**, 84 (2001).
- [15] S. M. Yusuf, A. Kumar, and J. V. Yakhmi, *Appl. Phys. Lett.* **95**, 182506 (2009).
- [16] I. L. Prejbeanu, M. Kerekes, R. C. Sousa, H. Sibuet, O. Redon, B. Dieny, and J. P. Nozières, *J. Phys.: Condens. Matter* **19**, 165218 (2007).
- [17] A. McDannald, C. R. dela Cruz, M. S. Seehra, and M. Jain, *Phys. Rev. B* **93**, 184430 (2016).
- [18] A. P. G. Rodrigues, M. A. Morales, R. B. Silva, D. R. A. B. Lima, R. L. B. A. Medeiros, J. H. Araújo, and D. M. A. Melo, *J. Phys. Chem. Solids* **141**, 109334 (2020).
- [19] P. Gupta and D. Pal, *J. Phys.: Condens. Matter* **33**, 135806 (2021).
- [20] A. Kumar, S. K. Giri, T. K. Nath, C. Ritter, and S. M. Yusuf, *J. Appl. Phys.* **128**, 203901 (2020).
- [21] Deepak, A. Kumar, and S. M. Yusuf, *Phys. Rev. Materials* **5**, 124402 (2021).
- [22] T. Bora and S. Ravi, *J. Appl. Phys.* **116**, 063901 (2014).
- [23] K. Yoshii, *Appl. Phys. Lett.* **99**, 142501 (2011).
- [24] Deepak, A. Kumar, and S. M. Yusuf, *J. Appl. Phys.* **127**, 213903 (2020).
- [25] K. Yoshii, N. Ikeda, Y. Shimojo, and Y. Ishii, *Mater. Chem. Phys.* **190**, 96 (2017).
- [26] H. M. Rietveld, *J. Appl. Crystallogr.* **2**, 65 (1969).
- [27] J. Rodríguez-Carvajal, *Physica B* **192**, 55 (1993).
- [28] See Supplemental Material at <http://link.aps.org/supplemental/10.1103/PhysRevMaterials.6.074405> for Rietveld refined x-ray diffraction patterns of $x = 0, 0.25, 0.5, 0.75$, and 1 compounds, SEM and EDX of $x = 0.25, 0.5$, and 0.75 compositions, Structural parameters viz. atomic position, bond length, bond angle and lattice constant variation with x derived from the Rietveld refinement of ND patterns at 300 K and low temperatures, respectively, and the ionic radii dependence of T_N for $R_{1-x}R'_x\text{CrO}_3$ compounds.
- [29] K. Yoshii and A. Nakamura, *J. Solid State Chem.* **155**, 447 (2000).
- [30] A. Durán, R. Escamilla, R. Escudero, F. Morales, and E. Verdín, *Phys. Rev. Materials* **2**, 014409 (2018).
- [31] K. Yoshii, *J. Appl. Phys.* **126**, 123904 (2019).
- [32] M. Ghanathe, A. Kumar, and S. M. Yusuf, *J. Appl. Phys.* **125**, 093903 (2019).
- [33] O. Halpern and T. Holstein, *Phys. Rev.* **59**, 960 (1941).
- [34] S. M. Yusuf, M. Sahana, K. Dörr, U. K. Röbler, and K. H. Müller, *Phys. Rev. B* **66**, 064414 (2002).
- [35] M. Ghanathe, A. Kumar, I. da Silva, and S. M. Yusuf, *J. Magn. Magn. Mater.* **523**, 167632 (2021).
- [36] A. Kumar and S. M. Yusuf, *J. Appl. Phys.* **121**, 223903 (2017).
- [37] M. Patra, S. Sabyasachi, S. Majumdar, S. Giri, A. Kumar, S. M. Yusuf, and V. Siruguri, *Mater. Res. Express* **1**, 036109 (2014).
- [38] A. Singh, R. Chatterjee, S. K. Mishra, P. S. R. Krishna, and S. L. Chaplot, *J. Appl. Phys.* **111**, 014113 (2012).
- [39] A. K. Bera and S. M. Yusuf, *J. Phys. Chem. C* **124**, 4421 (2020).
- [40] K. Yoshii and N. Ikeda, *J. Alloys Compd.* **804**, 364 (2019).
- [41] B. V. Prasad, G. N. Rao, J. W. Chen, and D. S. Babu, *Mater. Chem. Phys.* **126**, 918 (2011).
- [42] K. S. Cole and R. H. Cole, *J. Chem. Phys.* **9**, 341 (1941).
- [43] M. Coşkun, Ö. Polat, F. M. Coşkun, Z. Durmuş, M. Çağlar, and A. Türit, *J. Alloys Compd.* **740**, 1012 (2018).
- [44] A. Kahouli, A. Sylvestre, F. Jomni, B. Yangui, and J. Legrand, *J. Phys. Chem. A* **116**, 1051 (2012).
- [45] A. Bandarenka and G. A. Ragoisha, in *Inverse Problem in Potentiodynamic Electrochemical Impedance Spectroscopy* (Nova Science Publishers, Hauppauge, NY, 2005), p. 89.
- [46] K. Ben Brahim, M. Ben gzaïel, A. Oueslati, F. Hlel, and M. Gargouri, *Mater. Res. Bull.* **118**, 110505 (2019).
- [47] B. Zhang, Q. Zhao, A. Chang, Y. Li, Y. Liu, and Y. Wu, *Appl. Phys. Lett.* **104**, 102109 (2014).
- [48] S. Sharma, T. Basu, A. Shahee, K. Singh, N. P. Lalla, and E. V. Sampathkumaran, *J. Alloys Compd.* **663**, 289 (2016).
- [49] E. Niwa, T. Sato, Y. Watanabe, Y. Toyota, Y. Hatakeyama, K. Judai, K. Shozugawa, M. Matsuo, and T. Hashimoto, *J. Ceram. Soc. Jpn.* **123**, 501 (2015).
- [50] B. Udeshi, H. Boricha, B. Rajyaguru, K. Gadani, K. N. Rathod, D. Dhruv, S. B. Kansara, R. K. Trivedi, D. D. Pandya, K. Asokan, P. S. Solanki, and N. A. Shah, *Ceram. Int.* **45**, 1098 (2019).
- [51] A. K. Jonscher, *J. Phys. D: Appl. Phys.* **32**, R57 (1999).
- [52] S. R. Elliott, *Adv. Phys.* **36**, 135 (1987).
- [53] A. Ghosh, *Phys. Rev. B* **42**, 5665 (1990).
- [54] L. M. Daniels, M. C. Weber, M. R. Lees, M. Guennou, R. J. Kashtiban, J. Sloan, J. Kreisel, and R. I. Walton, *Inorg. Chem.* **52**, 12161 (2013).

- [55] D. K. S. Dimitrovska-Lazova, S. Aleksovska, M. Marinšek, and P. Tzvetkov, *Journals of Chemistry Bulgarian Academy of Sciences* **44**, 37 (2012).
- [56] I. Dzyaloshinsky, *J. Phys. Chem. Solids* **4**, 241 (1958).
- [57] A. H. Cooke, D. M. Martin, and M. R. Wells, *J. Phys. C: Solid State Phys.* **7**, 3133 (1974).
- [58] Y. Du, Z. X. Cheng, X.-L. Wang, and S. X. Dou, *J. Appl. Phys.* **108**, 093914 (2010).
- [59] J. Prado-Gonjal, R. Schmidt, J.-J. Romero, D. Ávila, U. Amador, and E. Morán, *Inorg. Chem.* **52**, 313 (2013).
- [60] M. Taheri, F. S. Razavi, Z. Yamani, R. Flacau, C. Ritter, S. Bette, and R. K. Kremer, *Phys. Rev. B* **99**, 054411 (2019).
- [61] L. F. Mendivil, J. Alvarado-Rivera, E. Verdín, J. A. Díaz, J. Mata, A. Conde, and A. Durán, *Appl. Phys. A* **126**, 574 (2020).
- [62] H. Zhang, J. Wang, L. Xie, D. Fu, Y. Guo, and Y. Li, *J. Appl. Phys.* **122**, 204103 (2017).
- [63] H. Wang, X. Liu, L. Hao, X. Ma, W. Han, K. Sun, D. Chen, H. Guo, Z. Fu, C.-W. Wang, P. Zhu, and Y. Liu, *J. Magn. Magn. Mater.* **473**, 428 (2019).
- [64] J. Shi, S. Yin, M. S. Seehra, and M. Jain, *J. Appl. Phys.* **123**, 193901 (2018).
- [65] V. K. Tripathi and R. Nagarajan, *ACS Omega* **2**, 2657 (2017).
- [66] Z. Xiang, S. Ge, Y. Huang, W. Li, and Y. Cui, *Solid State Sci.* **89**, 100 (2019).
- [67] B. B. Dash and S. Ravi, *J. Magn. Magn. Mater.* **461**, 91 (2018).
- [68] S. Yin, M. S. Seehra, C. J. Guild, S. L. Suib, N. Poudel, B. Lorenz, and M. Jain, *Phys. Rev. B* **95**, 184421 (2017).
- [69] J. R. Jesus, F. Garcia, J. G. S. Duque, and C. T. Meneses, *J. Alloys Compd.* **779**, 577 (2019).
- [70] M. Pecovska-Gjorgjevich, S. Aleksovska, M. Marinšek, and S. Dimitrovska-Lazova, *J. Am. Ceram. Soc.* **97**, 3864 (2014).
- [71] S. Chanda, S. Saha, A. Dutta, B. Irfan, R. Chatterjee, and T. P. Sinha, *J. Alloys Compd.* **649**, 1260 (2015).